ISSN 1674-1056
http://cpb.iphy.ac.cn
http://iopscience.iop.org/cpb
中国物理 B
Chinese Physics
中国物理 Chinese Physics B

Probing the minigap in topological insulator-based Josephson junctions under radio frequency irradiation

Guang Yang(杨光)[1,2], Zhaozheng Lyu(吕昭征)[1,2], Xiang Zhang(张祥)[1,2], Fanming Qu(屈凡明)[1,3,4], Li Lu(吕力)[1,2,3,4,5]
Citation: Chin. Phys. B . 2019, 28(12): 127402 . **doi:** 10.1088/1674-1056/ab5211
Journal homepage: http://cpb.iphy.ac.cn; http://iopscience.iop.org/cpb

What follows is a list of articles you may be interested in

Topological superconductivity in a $Bi_2Te_3/NbSe_2$ heterostructure: A review

Hao Zheng(郑浩), Jin-Feng Jia(贾金锋)
Chin. Phys. B . 2019, 28(6): 067403 . **doi:** 10.1088/1674-1056/28/6/067403

0-π transition induced by the barrier strength in spin superconductor Josephson junctions

Wen Zeng(曾文), Rui Shen(沈瑞)
Chin. Phys. B . 2018, 27(9): 097401 . **doi:** 10.1088/1674-1056/27/9/097401

Spatially resolved gap closing in single Josephson junctions constructed on Bi_2Te_3 surface

Yuan Pang(庞远), Junhua Wang(王骏华), Zhaozheng Lyu(吕昭征), Guang Yang(杨光), Jie Fan(樊洁), Guangtong Liu(刘广同), Zhongqing Ji(姬忠庆), Xiunian Jing(景秀年), Changli Yang(杨昌黎), Li Lu(吕力)
Chin. Phys. B . 2016, 25(11): 117402 . **doi:** 10.1088/1674-1056/25/11/117402

Critical current density behaviors across a grain boundary inclined to current with different angles in $YBa_2Cu_3O_{7-\delta}$ bicrystal junctions

Tao Hua(花涛), Wei-Wei Xu(许伟伟), Zheng-Ming Ji(吉争鸣), Da-Yuan Guo(郭大元), Qing-Yun Wang(王青云), Xiang-Rong Ma(马湘蓉), Rui-Yu Liang(梁瑞宇)
Chin. Phys. B . 2016, 25(6): 067401 . **doi:** 10.1088/1674-1056/25/6/067401

Developing Josephson junction array chips for microvolt applications

Wenhui Cao(曹文会), Jinjin Li(李劲劲), Yuan Zhong(钟源), Yuan Gao(高原), Honghui Li(李红晖), Zengmin Wang(王曾敏), Qing He(贺青)
Chin. Phys. B . 2016, 25(5): 057401 . **doi:** 10.1088/1674-1056/25/5/057401

RAPID COMMUNICATION

Probing the minigap in topological insulator-based Josephson junctions under radio frequency irradiation*

Guang Yang(杨光)[1,2], Zhaozheng Lyu(吕昭征)[1,2], Xiang Zhang(张祥)[1,2], Fanming Qu(屈凡明)[1,3,4,†], and Li Lu(吕力)[1,2,3,4,5,‡]

[1] *Beijing National Laboratory for Condensed Matter Physics, Institute of Physics, Chinese Academy of Sciences, Beijing* 100190, *China*
[2] *School of Physical Sciences, University of Chinese Academy of Sciences, Beijing* 100049, *China*
[3] *Songshan Lake Materials Laboratory, Dongguan* 523808, *China*
[4] *CAS Center for Excellence in Topological Quantum Computation, University of Chinese Academy of Sciences, Beijing* 100190, *China*
[5] *Beijing Academy of Quantum Information Sciences, Beijing* 100193, *China*

(Received 11 August 2019; revised manuscript received 30 September 2019; published online 15 November 2019)

Recently, a contact-resistance-measurement method was developed to detect the minigap, hence the Andreev bound states (ABSs), in Josephson junctions constructed on the surface of three-dimensional topological insulators (3D TIs). In this work, we further generalize that method to the circumstance with radio frequency (rf) irradiation. We find that with the increase of the rf power, the measured minigap becomes broadened and extends to higher energies in a way similar to the rf power dependence of the outer border of the Shapiro step region. We show that the corresponding data of contact resistance under rf irradiation can be well interpreted by using the resistively shunted Josephson junction (RSJ) model and the Blonder–Tinkham–Klapwijk (BTK) theory. Our findings could be useful when using the contact-resistance-measurement method to study the Majorana-related physics in topological insulator-based Josephson junctions under rf irradiation.

Keywords: topological insulator, Josephson junction, contact-resistance-measurement method, radio frequency irradiation

PACS: 74.45.+c, 03.65.Vf, 85.25.Cp **DOI:** 10.1088/1674-1056/ab5211

1. Introduction

In 2008, Fu and Kane proposed that the superconducting proximity effect between an s-wave superconductor (S) and the surface of a three-dimensional (3D) topological insulator (TI) can induce p-wave-like superconductivity and host Majorana bound states (MBSs) in the vortex cores or in the proximity-type S–TI–S Josephson trijunctions.[1] In more detail, the electron-like and hole-like Andreev bound states (ABSs) in single S–TI–S Josephson junctions are predicted to have 4π-period energy phase relations (EPRs), and the 1D Majorana edge modes are predicted to be fully decoupled when the phase difference reaches π, resulting in the complete close of minigap between the electron-like and hole-like ABSs. In Josephson trijunctions on 3D TIs, furthermore, MBS is predicted to exist at the center of the trijunction over extended regions in phase space. In the last years, experimental efforts have been paid to search for 4π-period current phase relations (CPRs), which are direct consequences of 4π-period EPRs. Some signatures, such as skewed CPR,[2–4] missing of odd Shapiro steps,[5–8] etc., have been discovered. Meanwhile, a contact-resistance-measurement method has also been developed for directly probing the EPRs in the junction area.[9–11] A linear closing behavior of minigap as a signature of 4π-period EPRs in single S-TI-S junctions and the complete close of minigap at the center of the S–TI–S trijunctions as an evidence of MBS have been observed.[10,11]

To further study the fractional Josephson effect in which the missing of odd Shapiro steps[5–8] is regarded as a signature of MBS, one would require to perform the contact-resistance-measurement method in the presence of radio-frequency (rf) irradiation in order to obtain the information of EPR and MBS. More generally, since MBSs suffer poisoning from quasiparticle fluctuations, one would ultimately require fast braiding/fusion operations and fast readout of MBSs at μs or ns time scales in the future, in order to test their non-Abelian statistics and to perform quantum computation. However, at such a short time scale and in the radio/micro frequency range, it is unclear whether the contact-resistance-measurement method can still be applied to probe the minigap, hence the MBSs, in

*Project supported by the National Basic Research Program of China (Grant Nos. 2016YFA0300601, 2017YFA0304700, and 2015CB921402), the National Natural Science Foundation China (Grant Nos. 11527806, 91221203, 11174357, 91421303, and 11774405), and the Strategic Priority Research Program B of the Chinese Academy of Sciences (Grant Nos. XDB07010100 and XDB28000000), and the Beijing Municipal Science & Technology Commission, China (Grant No. Z191100007219008).

†Corresponding author. E-mail: fanmingqu@iphy.ac.cn
‡Corresponding author. E-mail: lilu@iphy.ac.cn

© 2019 Chinese Physical Society and IOP Publishing Ltd

the S–TI–S junctions. To clarify this issue, in this work we investigate the contact-resistance-measurement method in the presence of rf irradiation. We find that this method still works — the measured data of contact resistance under rf irradiation can be well understood and numerically simulated by using the resistively shunted Josephson junction (RSJ) model[12] and the Blonder–Tinkham–Klapwijk (BTK) theory.[13]

2. Experiment

Figure 1(a) shows the false-color scanning electron microscopy (SEM) image of the device. The two superconducting Al electrodes couple with each other through a Bi_2Te_3 flake ($\sim$100 nm thick) to form a Josephson junction of length $L \sim 153$ nm and width $W \sim 484$ nm. The surfaces of the Al electrodes were oxidized *in situ* after deposition. An additional insulating layer of overexposed polymethyl methacrylate (PMMA) was fabricated to cover the device except for a window at the junction area (marked by the dashed rectangle in Fig. 1(a)). Through this window, a normal-metal Pd electrode was further deposited to electrically contact with the TI surface in the junction area for contact resistance measurement. Figure 1(b) shows the schematics of the device, together with the configurations for measurements of Josephson supercurrent (blue circuits) and contact resistance (yellow circuits). The measurements were carried out in a dilution refrigerator with a base temperature of $\sim$ 10 mK. The rf irradiation was applied via a coaxial cable with an open end as an antenna near the device.

In the following, we will first present and discuss the I_J–V_J curves (where I_J is the current passing from one superconducting electrode to another, and V_J is the voltage drop across the Josephson junction), and then present and discuss the data of contact resistance between the Pd electrode and Bi_2Te_3 under rf irradiation.

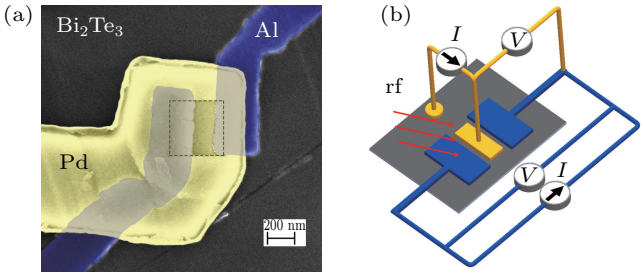


Fig. 1. Device structure and measurement configuration. (a) False-color SEM image of the proximity-type Josephson junction. A Josephson junction with Al electrodes (blue) was fabricated on the surface of a Bi_2Te_3 flake (gray, the whole image). The normal-metal Pd electrode (yellow) was deposited to contact the junction area through a window (marked by the dashed rectangle) on the insulating mask made of overexposed PMMA. Note that the surfaces of the Al electrodes were oxidized *in situ* before evaporating Pd. (b) Schematics of the device under rf irradiation. The configurations for measurements of contact resistance (yellow) and for Josephson supercurrent (blue) are illustrated.

3. Results and discussion

In the presence of rf irradiation, it is known that there will be Shapiro steps on the I_J–V_J curves of a Josephson junction.[12] Figure 2(a) shows the measured differential resistance dV_J/dI_J as a function of I_J and rf power P_{rf} applied to the antenna. Figure 2(b) shows the same data as in Fig. 2(a), but converted and replotted as a function of V_J and P_{rf}. The horizontal lines correspond to well defined Shapiro steps in the I_J–V_J curves at voltages $V_{Jn} = nhf_{rf}/2e = n \times 1.04$ μV, where h is the Planck constant, $f_{rf} = 0.5$ GHz is the rf frequency, e is the electron charge, and $n = 0, \pm1, \pm2, \ldots$

Usually, the Josephson supercurrent has a 2π-period CPR, which leads to the appearance of ordinary Shapiro steps on the I_J–V_J curves in the presence of rf irradiation. If the supercurrent contains a 4π-period component, however, the odd Shapiro steps might disappear, leading to the so called fractional Josephson effect.[14] In some S–TI–S junctions, the missing of the odd Shapiro steps has been observed.[5–7] In our devices, however, figure 2(b) shows that all the Shapiro steps are present. It indicates that the dominant supercurrent in our devices has a 2π-period CPR, flowing presumably through the bulk of the Bi_2Te_3 flake,[10] and that the 4π-period component of supercurrent in our device is negligibly small.

The I_J–V_J curves under rf irradiation can be simulated by solving the following equation based on the RSJ model:[12]

$$I_J + I_{rf0}\sin(2\pi f_{rf}t) = I_c\sin(\phi(t)) + \frac{d\phi(t)}{dt} \times \frac{1}{4\pi eR}, \qquad (1)$$

where I_J is the direct current, $I_{rf0} \propto \sqrt{P_{rf}}$ is the amplitude of the alternating current caused by the rf irradiation (the proportional constant can be determined from fitting the functional form to the experimental data), $I_c = 3.46$ μA is the critical supercurrent, $\phi(t)$ is the superconducting phase difference, and $R = 2.8\ \Omega$ is the resistance of the junction in the normal state. The details of our numerical simulation can be found in the supplementary materials. Figure 2(c) shows the simulated P_{rf} and I_J dependence of dV_J/dI_J. The result reproduces the main features of the experimental data in Fig. 2(a).

With increasing rf power, the region containing Shapiro steps in Fig. 2 extends to higher currents/voltages. The border of this region roughly coincides with the red dashed curve in Fig. 2(d) which represents the sum of the critical supercurrent I_c (the black line) and the amplitude of the rf-driving current I_{rf0}. It reflects that the Josephson junction can still have the chance to mode-lock with the rf driving frequency (i.e., forming the Shapiro steps), as long as the total bias current $I_J + I_{rf0}\sin(2\pi f_{rf}t)$ has the chance to be smaller than the critical supercurrent I_c within each oscillation period.[14]

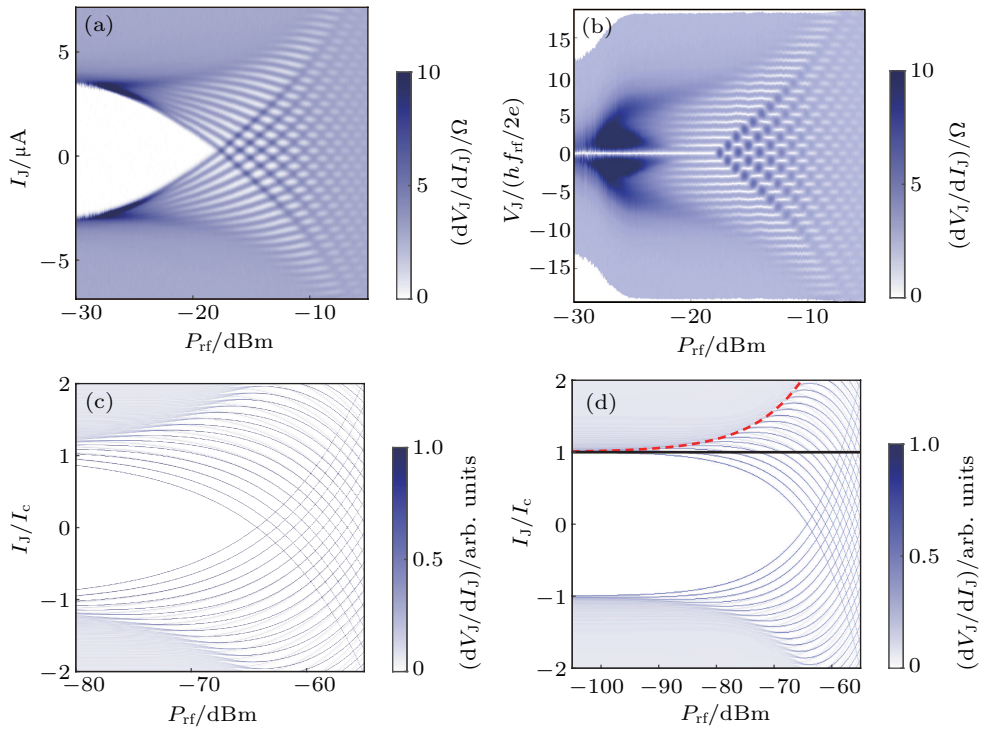


Fig. 2. Shapiro maps in an Al–Bi_2Te_3–Al junction. (a) Differential resistance dV_J/dI_J as a function of rf power P_{rf} and direct bias current I_J, measured at rf frequency $f_{rf} = 0.5$ GHz. (b) The same data as in (a), but replotted as a function of rf power P_{rf} and direct voltage V_J across the junction in units of $hf_{rf}/2e$. Evenly spaced Shapiro steps can be seen. (c) Simulated dV_J/dI_J based on the RSJ model. (d) The same simulated dV_J/dI_J as shown in (c), but in a wider range of rf power. The black line represents the critical supercurrent I_c, and the red curve represents the sum of the critical supercurrent I_c and the amplitude of the rf-driving current I_{rf0}.

In the next, let us present and discuss the data of the contact resistance dV_b/dI_b across the Pd–Bi_2Te_3 interface. Figure 3(a) shows the dV_b/dI_b as a function of rf power P_{rf} and bias current I_b. The vertical line cuts in Fig. 3(a) at low rf powers take basically the same line shape as the red curve ($P_{rf} = 0$) shown in Fig. 3(b), with a superconductivity-related dip–peak–dip structure due to the existence of a minigap on the TI surface of the S–TI–S junction.[10] Such a line shape can be well understood within the framework of the BTK theory.[10,13] The black curve in Fig. 3(b) is the BTK fitting to the experimental data, with fitting parameters as follows: the minigap $\Delta_0 = 20.4$ μeV, the effective number of channels of the contact $N = 25.5$, the barrier strength $Z = 0.66$, and the effective electron temperature $T = 0.1$ K. The standard error between the measured dV_b/dI_b (black) and the fitting curve (red) in Fig. 3(b) $\mathrm{SE} = \sqrt{\sum_{i=1}^{M}(y_{mi} - y_{fi})/M} = 25.7\ \Omega$, where $M = 501$ is the number of data points in Fig. 3(b), y_{mi} and y_{fi} are the measured and the fitted dV_b/dI_b at I_b of index i, respectively. The relative standard error is $\sim 25.7\ \Omega/720\ \Omega = 3.6\%$.

With increasing rf power P_{rf}, the dip–peak–dip structure on the vertical line cuts of Fig. 3(a), shown as the red curves in Fig. 3(d), gradually rounds up and spreads to higher I_b. The characteristic width of this structure, as indicated by the red dashed line in Fig. 3(c), follows a similar trace as the outer border of the Shapiro step regions in Fig. 2(a).

Theoretically, shining the device with rf irradiation will cause two effects on the contact resistance measurement. First, it will generate a rf current $I_{rf0}\sin(2\pi f_{rf}t)$ flowing mainly through the bulk of the junction, by which influencing the time-dependent phase difference $\phi(t)$ of the Josephson junction, thus influencing the minigap $\Delta(t)$. Second, the rf irradiation will also generate a rf current passing through the Pd–Bi_2Te_3 interface, by which modifying the contact resistance measurement. Combining these two effects, the contact resistance can be simulated as follows, still by using the RSJ model and the BTK theory.

In the presence of rf irradiation, the time-dependent minigap of the surface state should follow the 4π -period form[10] and can be expressed as $\Delta(t) = \Delta_0|\cos(\phi(t)/2)|$, where the time-dependent phase difference $\phi(t)$ can be obtained by solving Eq. (1). On the other hand, the time-dependent total bias current passing through the Pd–Bi_2Te_3 interface is $I_b + I'_{rf0}\sin(2\pi f_{rf}t)$, where I_b is the direct bias current and I'_{rf0} is the amplitude of the rf driving current (we set $I_{rf0}/I'_{rf0} = 14.4$ in order to fit the experimental data). We can extract the instant value of $dV_b(t)/dI_b(t)$ by using the fitting parameters Δ_0, N, Z, and T obtained before. Then, the time average of $dV_b(t)/dI_b(t)$, dV_b/dI_b, can be numerically obtained. The details of the simulation can be found in the supplementary materials. The simulated results are plotted in Fig. 3(c) and also as the black curves in Fig. 3(d) at several different rf powers. The red dashed line in Fig. 3(c) represents the border of

$I_b \leqslant I_e + I'_{rf0}$, where I_e is a characteristic current beyond which there is no signature of superconductivity without rf irradiation. It can be seen that the rf driving current makes the measured minigap structure extend to higher bias current under rf irradiation. Nevertheless, the numerical simulations can still reproduce the measured data.

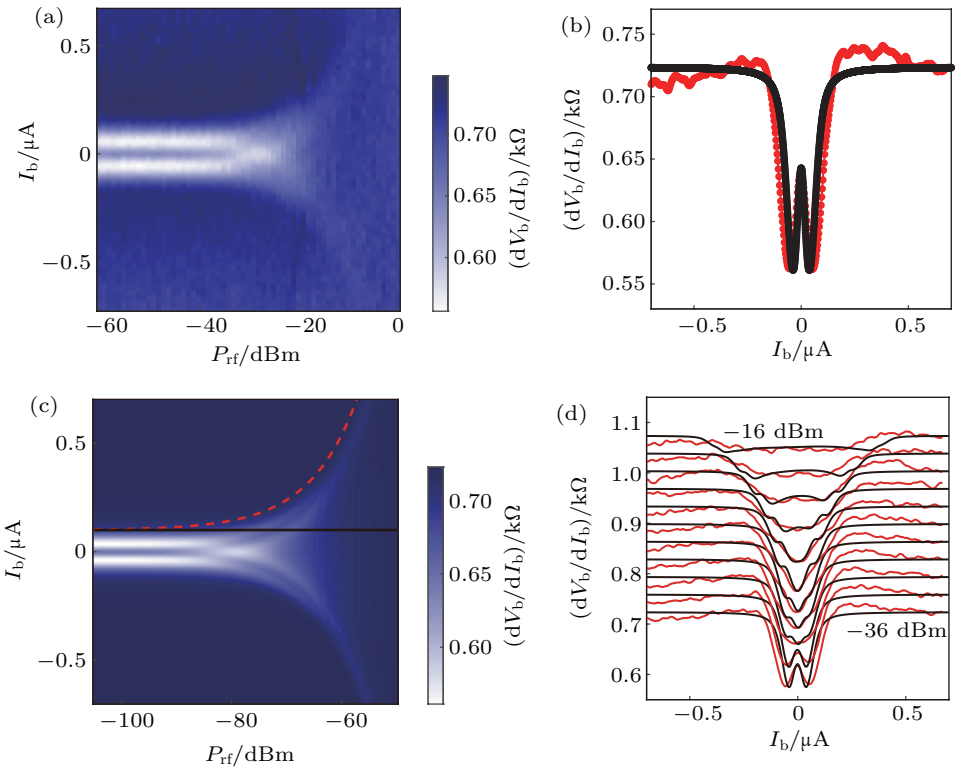


Fig. 3. Differential contact resistance in the junction. (a) The differential contact resistance dV_b/dI_b across the Pd–Bi_2Te_3 interface as a function of rf power P_{rf} and bias current I_b. (b) The dV_b/dI_b as a function of bias current I_b in the absence of rf irradiation (red curve), together with the BTK fitting (black curve). (c) The dV_b/dI_b calculated from the RSJ model and the BTK theory. The black line represents a characteristic current I_e at zero rf power, beyond which the signature of superconductivity disappears. The red dashed line represents the sum of I_e and the amplitude of the rf driving alternating current I'_{rf0} across the Pd–Bi_2Te_3 interface. (d) The rf power dependence of the measured dV_b/dI_b–I_b curves (red, from −36 dBm to −16 dBm) and the simulated ones (black) (curves are shifted vertically for clarity).

4. Conclusion

To conclude, we have examined and confirmed the validity of the contact-resistance-measurement method for detecting the minigap in S–TI–S Josephson junction under rf irradiation. Although both the phase difference across the Al–Bi_2Te_3–Al junction and the minigap measurement process across the Pd–Bi_2Te_3 interface are influenced by the rf irradiation, the measured contact resistance can still be interpreted by using the RSJ model and the BTK theory. These results might be useful when using the contact-resistance-measurement method to study the minigap of S–TI–S junctions under rf irradiation and Majorana-related physics.

References

[1] Fu L and Kane C L 2008 *Phys. Rev. Lett.* **100** 096407

[2] Sochnikov I, Maier L, Watson C A, Kirtley J R, Gould C, Tkachov G, Hankiewicz E M, Brüne C, Buhmann H, Molenkamp L W and Moler K A 2015 *Phys. Rev. Lett.* **114** 066801

[3] Kurter C, Finck A D K, Hor Y S and Van Harlingen D J 2015 *Nat. Commun.* **6** 7130

[4] Kayyalha M, Kazakov A, Miotkowski I, Khlebnikov S, Rokhinson L P and Chen Y P 2018 arXiv:1812.00499

[5] Rokhinson L P, Liu X and Furdyna J K 2012 *Nat Phys.* **8** 795

[6] Wiedenmann J, Bocquillon E, Deacon R S, Hartinger S, Herrmann O, Klapwijk T M, Maier L, Ames C, Brüne C, Gould C, Oiwa A, Ishibashi K, Tarucha S, Buhmann H and Molenkamp L W 2016 *Nat. Commun.* **7** 10303

[7] Bocquillon E, Deacon R S, Wiedenmann J, Leubner P, Klapwijk T M, Brune C, Ishibashi K, Buhmann H and Molenkamp L W 2017 *Nat. Nanotechnol.* **12** 137

[8] Le Calvez K, Veyrat L, Gay F, Plaindoux P, Winkelmann C B, Courtois H and Sacépé B 2019 *Commun. Phys.* **2** 4

[9] Pang Y, Wang J, Lyu Z, Yang G, Fan J, Liu G, Ji Z, Jing X, Yang C and Lu L 2016 *Chin. Phys. B* **25** 117402

[10] Lyu Z, Pang Y, Wang J, Yang G, Fan J, Liu G, Ji Z, Jing X, Yang C, Qu F and Lu L 2018 *Phys. Rev. B* **98** 155403

[11] Yang G, Lyu Z, Wang J, Ying J, Zhang X, Shen J, Liu G, Fan J, Ji Z, Jing X, Qu F and Lu L 2019 arXiv:1904.02677

[12] Barone A and Paterno G 1982 *Physics and Application of the Josephson Effect* (New York: John Wiley and Sons) p. 122

[13] Blonder G E, Tinkham M and Klapwijk T M 1982 *Phys. Rev. B* **25** 4515

[14] Domínguez F, Kashuba O, Bocquillon E, Wiedenmann J, Deacon R S, Klapwijk T M, Platero G, Molenkamp L W, Trauzettel B and Hankiewicz E M 2017 *Phys. Rev. B* **95** 195430